AGU PUBLICATIONS

JGR

Journal of Geophysical Research: Oceans

RESEARCH ARTICLE

10.1002/2017JC013609

Key Points:
- High-frequency weather systems strongly lower the daily-mean SST and damp its variability with little effect on SST diurnal variability
- The impact of high-frequency weather systems on SST is strongly regulated by the background mixed layer depth
- The impact of high-frequency weather systems on the central Arabian Sea is due primarily to high-frequency wind fluctuations

Correspondence to:
S. Zhou,
Shenjie.Zhou@uea.ac.uk

Citation:
Zhou, S., Zhai, X., & Renfrew, I. A. (2018). The impact of high-frequency weather systems on SST and surface mixed layer in the central Arabian Sea. *Journal of Geophysical Research: Oceans*, *123*, 1091–1104. https://doi.org/10.1002/2017JC013609

Received 6 NOV 2017
Accepted 15 JAN 2018
Accepted article online 19 JAN 2018
Published online 9 FEB 2018

© 2018. American Geophysical Union. All Rights Reserved.

The Impact of High-Frequency Weather Systems on SST and Surface Mixed Layer in the Central Arabian Sea

Shenjie Zhou[1], Xiaoming Zhai[1], and Ian A. Renfrew[1]

[1]Centre for Ocean and Atmospheric Sciences, School of Environmental Sciences, University of East Anglia, Norwich, United Kingdom

Abstract The role of high-frequency (subdaily time scales) weather systems in modulating the sea surface temperature (SST) and the mixed layer (ML) depth in the central Arabian Sea is investigated using one-dimensional mixed-layer models for different monsoon seasons. Simulations forced by subhourly sampled meteorological variables, including surface wind, air temperature, humidity, and cloud, are compared to simulations forced by daily-averaged meteorological variables. It is found that including high-frequency signals in the meteorological variables lowers the daily-mean SST (by 0.8°C on average) and damps its variability (the standard deviation decreases by 1.0°C) but has little systematic effect on the SST diurnal variability. There is a small but consistent deepening of the ML depth associated with the slightly intensified wind stress and heat loss due to high-frequency weather systems at this site. The cooling effect on the daily-mean SST is found to be closely related to the ML depth on daily-to-seasonal time scales. The impact of high-frequency weather systems is primarily driven by the high-frequency wind via the turbulent heat and momentum fluxes.

1. Introduction

Variability in air-sea fluxes on subdaily time scales has been recognized as important in perturbing sea surface temperature (SST) and forcing changes in climate variability. For example, previous studies show that diurnal variations in solar radiation lead to a diurnal cycle in SST (e.g., Shinoda, 2005; Shinoda & Hendon, 1998); and this diurnal cycle in the SST causes warmer daily-mean and intraseasonal-mean SST, referred as the rectification effect of the SST diurnal cycle (Bernie et al., 2005). The impact of high-frequency atmospheric forcing on low-frequency SST variation can further influence long-term atmosphere-ocean phenomena such as the Madden-Julian Oscillation (e.g., Bernie et al., 2007, 2008), the Intraseasonal Oscillation (e.g., Ham et al., 2014; Hu et al., 2015), and the El Niño-Southern Oscillation (ENSO; e.g., Danabasoglu et al., 2006; Terray et al., 2012).

Most modeling studies that examine the impact of atmospheric forcing on subdaily time scales have done so by filtering the surface turbulent and radiative fluxes. Few studies have filtered the meteorological variables. Owing to the nonlinear dependence of air-sea fluxes on meteorological variables, high-frequency fluctuations in meteorological variables such as surface wind and air temperature not only cause air-sea fluxes to vary at high frequencies but also contribute significantly toward the low-frequency and time-mean air-sea momentum and energy fluxes (e.g., Gulev & Belyaev, 2012; Zhai et al., 2012; Zhai & Wunsch, 2013). Therefore, for the purpose of assessing the impact of weather systems on the ocean, filtering the meteorological variables, rather than air-sea fluxes, is the appropriate approach. A number of recent studies have investigated the impact of mesoscale and synoptic-scale weather systems on the ocean and found that the presence of weather systems (e.g., polar lows and topographic jets) strongly enhances heat loss in the subpolar North Atlantic, which leads to intense deep convection in convective areas (Condron et al., 2008; Våge et al., 2008), spinning-up the gyre circulation and strengthening the meridional overturning circulation (Condron & Renfrew, 2013; Holdsworth & Myers, 2015; Jung et al., 2014; Wu et al., 2016). However, there have been few studies focusing on the composite impact of weather systems on subdaily time scales on the upper ocean, particularly at low latitudes, with the exception of specific studies on the impacts of tropical cyclones on the upper ocean (e.g., Bender et al., 1993; Dare & McBride, 2011; Price et al., 2008).

In this study, we use one-dimensional mixed-layer models to investigate the impact of weather systems on subdaily time scales on the SSTs and mixed-layer (ML) depth in a monsoon-dominated tropical sea, the

central Arabian Sea, taking advantage of the comprehensive observational data available at this site (Weller et al., 1998). In particular, we compare model simulations forced by subhourly sampled meteorological variables, including surface wind, air temperature, humidity, and cloud amount, to simulations forced by variables that have been filtered. Additional sensitivity experiments are also conducted to pin down the key meteorological variable(s) and their impacts on subdaily time scales in the central Arabian Sea.

2. Data and Methods

2.1. Observations

Our meteorological observations are a yearlong (16 October 1994 to 19 October 1995) time series of surface 10 m zonal and meridional wind velocities, air and sea surface temperatures, relative humidity, barometric air pressure, downwelling shortwave and longwave radiation, and precipitation rate recorded every 7.5 min by a moored meteorological measurement package deployed off the Omani coast (15.5°N, 61.5°E; Figure 1) in the central Arabian Sea. Colocated subsurface oceanic instruments attached on the mooring reached down to 300 m, and recorded temperature, salinity, and current velocities every 15 min. The atmospheric conditions at this site are dominated by three seasons (see Figures 2a and 2b): the northeast (NE) monsoon season (November 1994 to mid-February 1995) is characterized by moderate, cold, and dry northeasterly wind forcing, and oceanic heat loss; the intermonsoon season (mid-February 1995 to mid-June 1995) is dominated by weak wind events, allowing oceanic heat gain; and the southwest (SW) monsoon season (mid-June 1995 to mid-September 1995) features a strong southwesterly wind burst associated with the Findlater Jet (Findlater, 1977) blowing diagonally across the Arabian Sea, and summertime oceanic heat gain. A detailed introduction of this data set is covered in Weller et al. (1998), which confirms that the atmospheric conditions from 1994 to 1995 are generally typical for this site.

2.2. Experimental Design

The main simulations shown in this paper are conducted with the one-dimensional PWP model developed by Price et al. (1986). The PWP model simulates ML temperature and salinity via diffusion equations and three stability criteria: static stability, ML stability (bulk Richardson number ≤ 0.65), and shear flow stability (gradient Richardson number ≤ 0.25). The vertical resolution of the model is set to be 0.4 m in our experiments, which is sufficient to resolve the diurnally varying SST (Bernie et al., 2005).

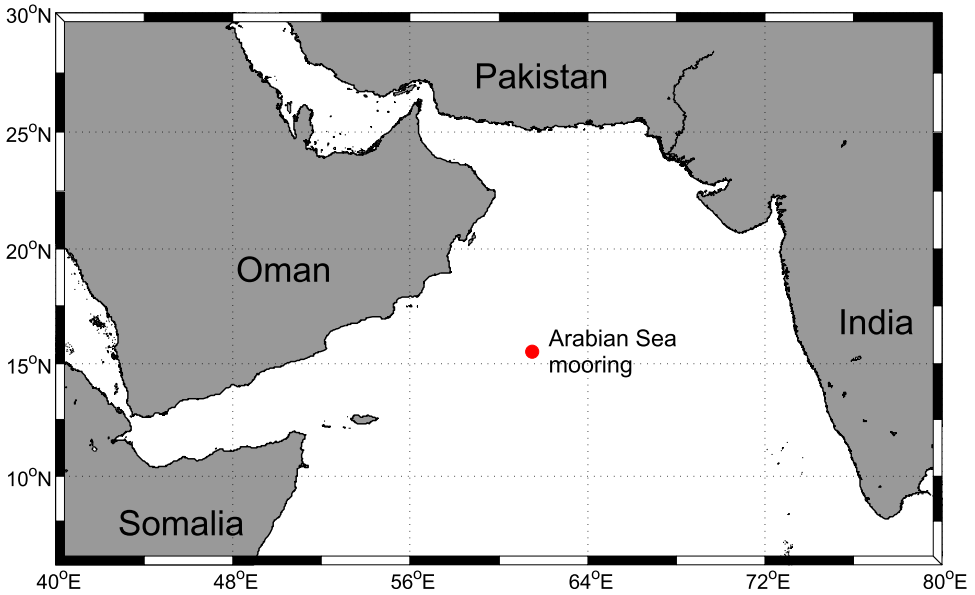

Figure 1. The Arabian Sea upper ocean dynamics mooring is located at 15.5°N, 61.5°E, as marked by the red circle. The location is on the climatological axis of the Findlater Jet and representative of the open ocean rather than coastal water.

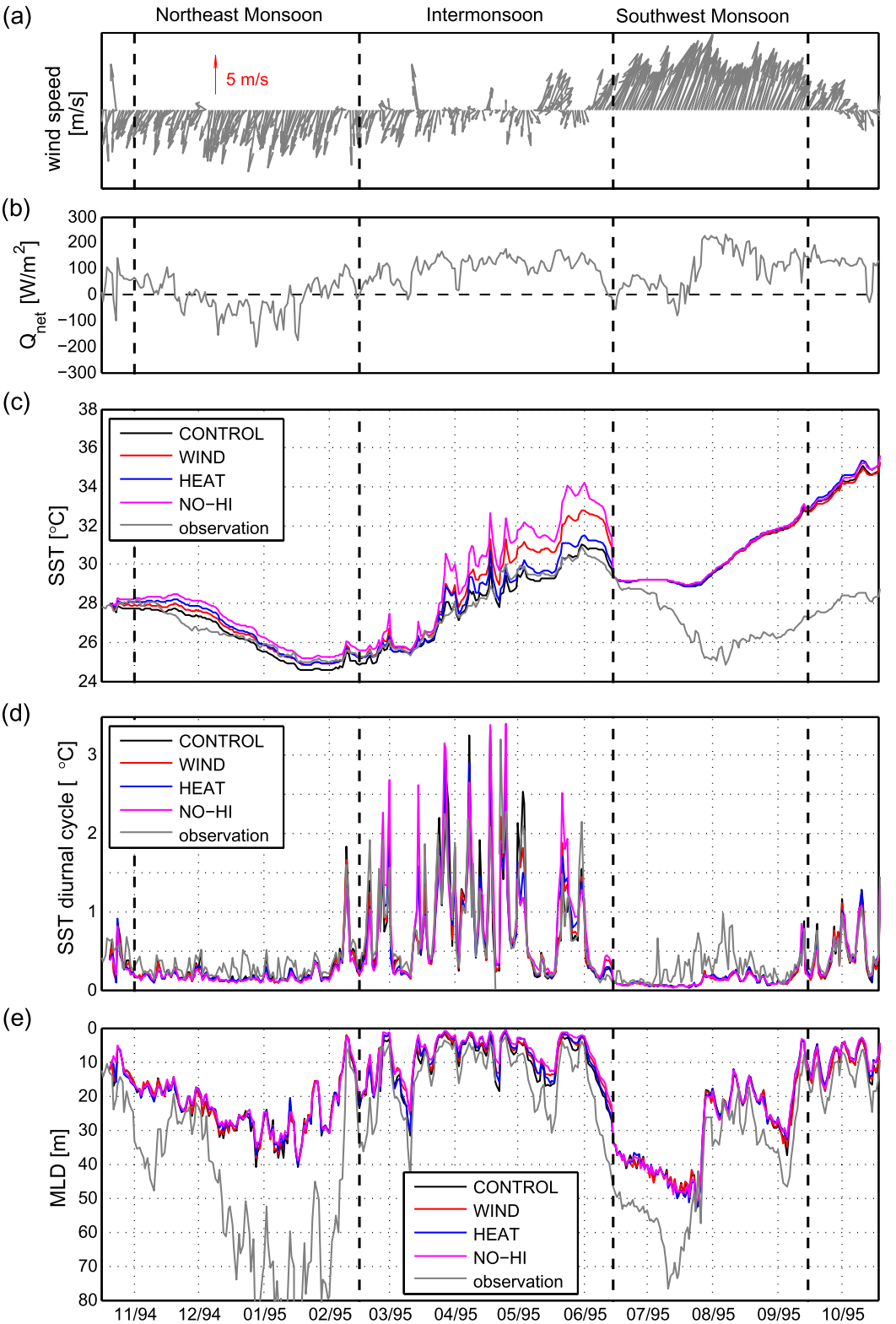

Figure 2. Yearlong time series of (a) wind speed, (b) daily-mean net surface heat flux, (c) daily-mean SST, (d) magnitude of SST diurnal variability, and (e) daily-mean ML depth. The wind speed is plotted with a coarse temporal resolution (half-daily) for clarity. The line colors show observations (grey) and simulations: CONTROL (black), WIND (red), HEAT (blue), and NO-HI (magenta).

We first conduct a control simulation (CONTROL) forced by air-sea fluxes calculated from the observed atmospheric variables at their original 7.5 min temporal resolution, using the COARE 3.0 bulk flux formulae (Fairall et al., 2003),

$$\begin{aligned} Q_{net}^{SW} &= Q^{SW}(1-\alpha), \\ Q_{net}^{LW} &= Q^{LW} - \varepsilon_{atm}\sigma(T_S)^4, \\ Q^{LH} &= \rho_{air} C_e L_e |\mathbf{U}|(q_{air} - q_{sat}), \\ Q^{SH} &= \rho_{air} C_h c_p |\mathbf{U}|(T_{air} - T_S), \\ Q_{net} &= Q_{net}^{SW} + Q_{net}^{LW} + Q^{LH} + Q^{SH}, \\ \tau &= \rho_{air} C_d |\mathbf{U}|\mathbf{U}, \end{aligned} \tag{1}$$

where Q_{net}^{SW} and Q_{net}^{LW} are the net shortwave and longwave radiation at sea surface, Q^{LH} and Q^{SH} are the latent and sensible heat fluxes, α is the albedo, C_e and C_h are the transfer coefficients for moisture and heat, respectively, c_p is the heat capacity of the dry air, L_e is the latent heat of vaporization, T_{air} and T_S are the observed surface air temperature and sea surface temperature, q_{air} and q_{sat} are the observed specific humidity and saturated humidity at T_S and P (barometric pressure), and C_d is the drag coefficient and $\mathbf{U}$ is the 10 m wind velocity. The effect of including surface ocean currents in the bulk formulae on turbulent air-sea momentum and heat fluxes is not considered here due to the lack of surface current measurements.

To isolate and quantify the influence of high-frequency atmospheric variability, we conduct three additional experiments. The WIND experiment is the same as CONTROL except that the surface turbulent and radiative heat fluxes are calculated from daily-averaged (24 h running mean) meteorological variables. The HEAT experiment is the same as CONTROL except that the surface wind stresses are calculated from daily-averaged winds. The NO-HI experiment is forced from both surface heat fluxes and wind stresses calculated with daily-average meteorological variables. In each experiment, the model is reinitialized at the beginning of each season as defined in section 2.1, which allows us to estimate the impact of the high-frequency atmospheric forcing under different meteorological conditions without being interfered by any potential model drift from the previous season. An alternative one-dimensional turbulence closure Kantha-Clayson (KC) model (Kantha & Clayson, 1994) has also been run with identical forcing and experimental design and it shows qualitatively the same results (see Appendix A).

2.3. Parameterization of Cloud Amount

The cloud amount (C) is not directly observed, yet it plays a crucial role in regulating the downwelling shortwave and longwave radiation. In previous studies of weather's impact on the ocean (e.g., Condron & Renfrew, 2013; Wu et al., 2016), perturbing the cloud amount has not been considered. Here its role on the radiative fluxes is examined. To determine the effect of high-frequency (subdaily time scale) cloud variability on surface radiative heat fluxes, C has to be determined. To do so, we use parameterizations of C based on empirical relationships between cloudiness and downwelling radiation.

First, C can be calculated from the observed shortwave radiation (Q^{SW}) and the (theoretical) clear-sky shortwave radiation (Q_{clr}^{SW}) according to Reed (1977):

$$\frac{Q^{SW}}{Q_{clr}^{SW}} = 1 - 0.62C + 0.0019(90 - Z), \tag{2}$$

where C is the fraction of cloud cover and Z is the solar zenith angle in degrees. The clear-sky shortwave radiation determination is based on ASCE-EWRI (2005).

Second, cloud cover also affects the downwelling longwave radiation according to Zillman (1972):

$$Q^{LW} = Q_{clr}^{LW} + 0.96C\sigma T_{air}^4(1 - 9.2\times10^{-6}T_{air}^2), \tag{3}$$

where Q^{LW} is the observed downwelling longwave radiation, Q_{clr}^{LW} is the clear-sky downwelling longwave radiation, T_{air} is the air temperature in Kelvin, and $\sigma = 5.67\times10^{-8}$ W m^{-2} K^{-4} is the Stefan-Boltzmann coefficient. The clear-sky longwave radiation can be determined following:

Table 1
Root-Mean-Square Error (RMSE) and Mean Bias Deviation (MBD) Are Calculated Between the Observed Radiative Fluxes and the Calculated Radiative Fluxes With the "Hybrid" and "Longwave-Only" Cloud Scheme, for Different Clear-Sky Emissivity Schemes as Summarized by Gubler et al. (2012*)*

	"Hybrid" versus observations		"Longwave-only" versus observations	
ε_{atm} scheme	RMSE (W/m^2)	MBD (W/m^2)	RMSE (W/m^2)	MBD (W/m^2)
Maykut and Church (1973)	31.74	−14.02	112.37	−58.04
Ångström (1915)	25.98	−3.30	78.15	−19.08
Brunt (1932)	26.75	6.20	71.60	15.94
Swinbank (1963)	25.40	1.48	66.78	−2.58
Idso and Jackson (1969)	25.77	3.88	64.90	4.95
Brutsaert (1975)	29.59	13.44	77.37	30.45
Konzelmann et al. (1994)	27.37	9.14	68.43	19.44
Satterlund (1979)	27.77	9.92	69.05	20.02
Idso (1981)	48.91	38.77	118.96	69.62
Iziomon et al. (2003)	25.72	2.39	68.10	5.19
Prata (1996)	28.32	11.12	72.88	25.20
Dilley and O'Brien (1997)	**25.35**	**–0.52**	68.20	−5.11

Note. The best combination used for net surface heat flux recalculation is the "hybrid" cloud scheme and the emissivity scheme proposed by Dilley and O'Brien (1997).

$$Q_{clr}^{LW} = \varepsilon_{atm}\sigma T_{air}^4, \quad (4)$$

where ε_{atm} is the clear-sky emissivity which depends on water vapor pressure and air temperature.

During the day, C can be derived via (2) or (3), while during the night C can only be derived from (3). As such, two possible ways to determine C are tested: (a) the "longwave-only" C; (b) the "hybrid" C derived using (2) during the day and (3) during the night. Table 1 shows the root-mean-square errors (RMSEs) between the observed radiative heat fluxes and those calculated with either "hybrid" or "longwave-only" cloud scheme involved. In our study, the "hybrid" scheme is used to recalculate the radiative fluxes since on average RMSE associated with the "hybrid" scheme is only about one third of that associated with the "longwave-only" scheme. In addition, 12 parameterization schemes for ε_{atm} summarized in Gubler et al. (2012) were tested and the scheme proposed by Dilley and O'Brien (1997) was chosen since it provides the best fit in calculated net radiative fluxes compared to the observations (Table 1). With this parameterization of C, the subdaily cloud variability owing to weather systems can then be filtered out in sensitivity experiments such as WIND and NO-HI. It is worth pointing out that the diurnal solar forcing remains unaltered in all the experiments since it is a consequence of the Earth's rotation, rather than weather phenomena. Consequently, the above approach enables us to filter out all the meteorological signals associated with high-frequency weather systems without disrupting the solar cycle.

3. Results

3.1. Fidelity in Simulating SST and ML Depth

The PWP model only simulates the local response of oceanic properties to the surface heat and momentum fluxes without accounting for the lateral advection of heat. In this section, the results of the CONTROL experiment are compared with the observations to evaluate the suitability of the PWP model and address the relative importance of the horizontal processes in three different seasons. The interpretation of the results follows the separation of three seasons as marked by the vertical dashed lines in Figure 2.

3.1.1. Daily Mean

Figure 2c shows the daily-mean SST (black) simulated in CONTROL agrees reasonably well with the observed daily-mean SST (grey) during the NE monsoon and intermonsoon seasons while the CONTROL SST gradually drifts away from the observations at the onset of the SW monsoon season. Although there are some discrepancies between the CONTROL and observed daily-mean ML depth, the PWP model reproduces the overall seasonal trend of ML depth found in the observations—deep ML in the monsoon seasons and much shallower ML in the intermonsoon season (Figure 2e).

In the NE monsoon season, the agreement between the CONTROL daily-mean SST and observed daily-mean SST suggests that horizontal processes play a minor role in setting the SST evolution during this season. The CONTROL daily-mean ML deepens corresponding to the daily heat loss at the sea surface (Figure 2b) throughout December and January and shoals in response to the net surface heat gain and weaker wind events towards mid-February (Figures 2a and 2b), agreeing with the general trend of observed daily-mean ML depth. However, the observed daily-mean ML depth also shows a rapid deepening-shoaling-deepening trend from early November to late December, resulting from the changes in the thermocline structure caused by the passage of a pair of eddies at the mooring site as confirmed by concurrent altimetric SSH imagery (Fischer et al., 2002). An additional heat budget analysis conducted by Fischer et al. (2002) suggests that the horizontal heat advection is near-zero within the ML, which explains the agreement between the one-dimensionally forced SST and the observed SST in the NE monsoon season. Their heat budget analysis also shows a strong horizontal heat flux below the ML from November to early December due primarily to variations in the thermocline thickness associated with the mesoscale eddies (Fischer, 2000).

In the intermonsoon season, the simulated daily-mean SST and ML depth both agree well with the observations, indicating that the upper ocean variability during this time period is primarily surface driven. A heat and salt budget analysis based on the observations (Weller et al., 2002, Figures 12 and 13) demonstrate a one-dimensional balance during the intermonsoon season and confirm that horizontal processes have little effect on the intermonsoon SST and ML depth evolution.

In the SW monsoon season, the drift of simulated SST is coincident in time with a reported cool filament (Fischer et al., 2002) that developed from the Omani coast and moved offshore toward the mooring site. Influenced by this horizontal input of thermal variability, the observed daily-mean SST is much lower than that simulated by the PWP model (where the SST is only locally driven). Although the daily-mean SST in the SW monsoon season is strongly affected by horizontal processes, a better agreement on the daily-mean ML depth between simulation and observation (Figure 2e) suggests that the prevailing strong southwesterlies throughout the whole season are the primary local mechanism for the ML deepening and entrainment (Weller et al., 2002), and the strong surface heat gain during mid-July (Figure 2b) is responsible for the ML shoaling in both the observation and the simulation, while horizontal processes are not as significant in regulating the ML development as those in the NE monsoon season.

3.1.2. Subdaily Variability

On subdaily time scales, the PWP model performs well in reproducing the magnitude of SST diurnal variability as shown in Figure 2d. The observed SST diurnal variability (grey) is pronounced in the intermonsoon season (0.71°C on average) and relatively weak in both monsoon seasons (0.26°C in the NE monsoon season, 0.21°C in the SW monsoon season). This significant seasonal dependence of the magnitude of SST variability in the observations is reproduced in the CONTROL experiment (black), which is primarily determined by the distinct seasonal meteorological conditions in terms of the strength of the surface heating and the wind-driven mixing (e.g., Bernie et al., 2007). In particular, the surface heating forces the formation of a thin warm layer with a small heat capacity in the surface ocean during the daytime heating period, which leads to a rapid increase of the SST. The wind forcing, on the other hand, acts to inhibit the heating-driven stratification by inducing shear instability at the base of ML and the consequent mixing and entrainment processes suppress the increase of the SST during the day. The weaker SST diurnal variability in both monsoon seasons is mostly attributed to the strong monsoonal winds prevailing throughout the whole season, while the weak surface heating during the daytime also contributes to smaller SST diurnal oscillations in the NE monsoon season. For the intermonsoon season, strong solar heating and relatively calm winds are in favor of a greater SST diurnal cycle. It is noted that both the PWP model and the KC model predict the magnitude of SST diurnal variability in the SW monsoon season to be around 0.1°C, while in the observations the value exceeds 0.5°C from July to mid-August (Figures 2d and A1b). The underestimated SST diurnal variability is likely due to the lack of horizontal processes in the PWP model.

Comparisons with the observations show that the PWP model is able to simulate the daily-mean SST and ML depth, and the SST diurnal variability for most of the year. Results from the CONTROL experiment suggest that, at the Arabian Sea mooring site, the ML heat budget is mostly controlled by one-dimensional heat exchanges at both the air-sea interface and the base of the ML with the exception of some drift during the SW monsoon season. Nevertheless, the horizontal heat fluxes seem to affect the ML dynamics much less and the main drivers of the ML variability in the SW monsoon season, i.e., strong wind-driven shear instability and strong surface buoyancy-driven restratification, are well represented in the model. Despite some limitations in the SW monsoon season, overall the one-dimensional model setup provides a reasonably good simulation of SST and ML depth at our study site and is sufficiently good to warrant investigating a series of sensitivity simulations with varied atmospheric forcing.

3.2. Response of SST and ML Depth to High-Frequency Weather Systems

Figure 2 shows the SSTs and ML depths simulated by the four experiments. Comparing the results of the CONTROL (black) and the NO-HI (magenta) experiments suggests that including high-frequency weather systems in the atmospheric forcing systematically deepens the ML and significantly lowers the SST. On average, including high-frequency weather systems deepens the ML depth by 1.3 m and lowers the SST by 0.8°C in the CONTROL simulation compared to the NO-HI simulation. Particularly, the high-frequency weather systems lower the daily-mean SST more significantly in the intermonsoon season. Averaging over the entire season, the SST is lowered by 1.7°C in CONTROL compared to NO-HI, due to the inclusion of high-frequency variability in the atmospheric forcing. Furthermore, high-frequency (subdaily) weather systems

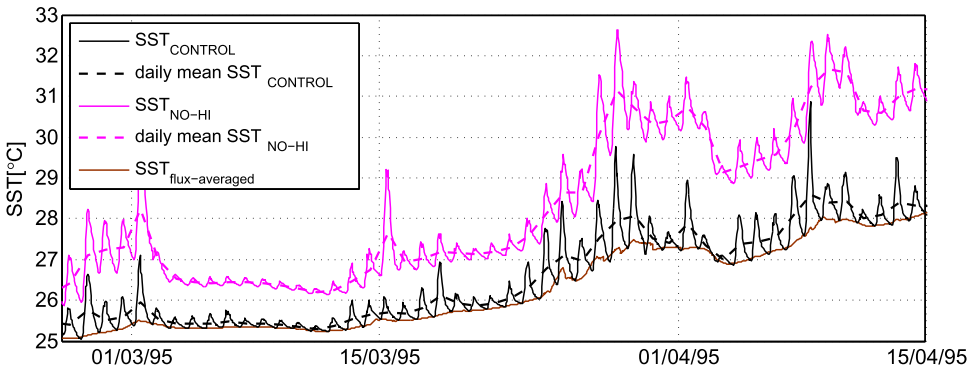

Figure 3. SST from the CONTROL (black) and the NO-HI (magenta) experiments, with daily-mean SST marked as dashed lines. The SST from an experiment forced by daily-averaged surface fluxes is shown as a brown line.

also damp the low-frequency (daily-mean) SST variability. For example, the standard deviation of daily-mean SST in the intermonsoon season is considerably weaker in the CONTROL experiment (1.9°C, close to 1.86°C in observation) than that in the NO-HI experiment (2.9°C). Results from WIND (red) and HEAT (blue) further show that high-frequency weather systems lower the daily-mean SST via their effect on turbulent momentum and heat fluxes, although their effect on turbulent heat fluxes appears to have a greater impact on the daily-mean SST (Figure 2c).

The difference between the approach of averaging meteorological variables used in the present study and the approach of averaging surface fluxes used in previous studies (e.g., Bernie et al., 2005; Shinoda, 2005; Shinoda & Hendon, 1998) is highlighted in Figure 3 for a 6 week period in the intermonsoon season. Averaging surface fluxes eliminates the diurnal cycle in SST and lowers the daily-mean SST by up to 0.85°C (0.2°C on average) due to the absence of the rectification effect of a thin warm surface layer formed during the day. In contrast, averaging meteorological variables is found to increase the daily-mean SST by as much as 3.7°C while still maintaining the diurnal cycle of SST. The total difference in SST between forcing with averaged meteorological variables and averaged fluxes is up to 4°C.

As shown in Figure 2 (see also Table A1), although high-frequency weather systems significantly lower the daily-mean SST, they have little systematic effect on the magnitude of the SST diurnal variability at our study site (Figure 2d). Both the magnitude of the SST diurnal variability and its seasonal dependence are similar in the four experiments and resemble the observations. The nonsystematically affected SST diurnal variability is likely to be attributed to the randomly distributed high-frequency cloud and wind over a 24 h composite window (see following section).

3.3. The Composite Analysis

Our model results have shown that the high-frequency atmospheric forcing lowers the SST and deepens the ML depth (Figures 2c–2e) much more significantly in the intermonsoon season than the monsoon seasons. To further examine this seasonal dependence of the response of upper ocean SST and ML depth to the high-frequency weather systems, we construct 24 h composites of surface fluxes, wind speed, SST, and ML depth for experiments CONTROL and NO-HI and the observations for each season (Figure 4).

Two main factors contribute to the much greater difference in SST between the CONTROL and the NO-HI experiments seen in the intermonsoon season (–1.83°C on seasonal average; Figure 4) than monsoon seasons (–0.71°C in the NE monsoon season and −0.11°C in the SW monsoon season). First, including high-frequency weather systems leads to a greater increase in wind speed (0.31 m/s) and surface heat loss in the intermonsoon season (–13.27 W/m^2 in total with −9.53 W/m^2 contributed by wind-related turbulent fluxes) compared to the other two seasons. This is mainly because the intermonsoon winds fluctuate more (blowing in different directions) than monsoonal winds which mostly blow in a uniform direction (NE monsoon blows southwestward and SW monsoon blows northeastward, see also Figure 2a) and high-frequency intermonsoon wind cancels out more significantly when the daily average is applied. Further analysis shows that the difference in net surface heat flux between CONTROL and NO-HI are explained mostly by the difference

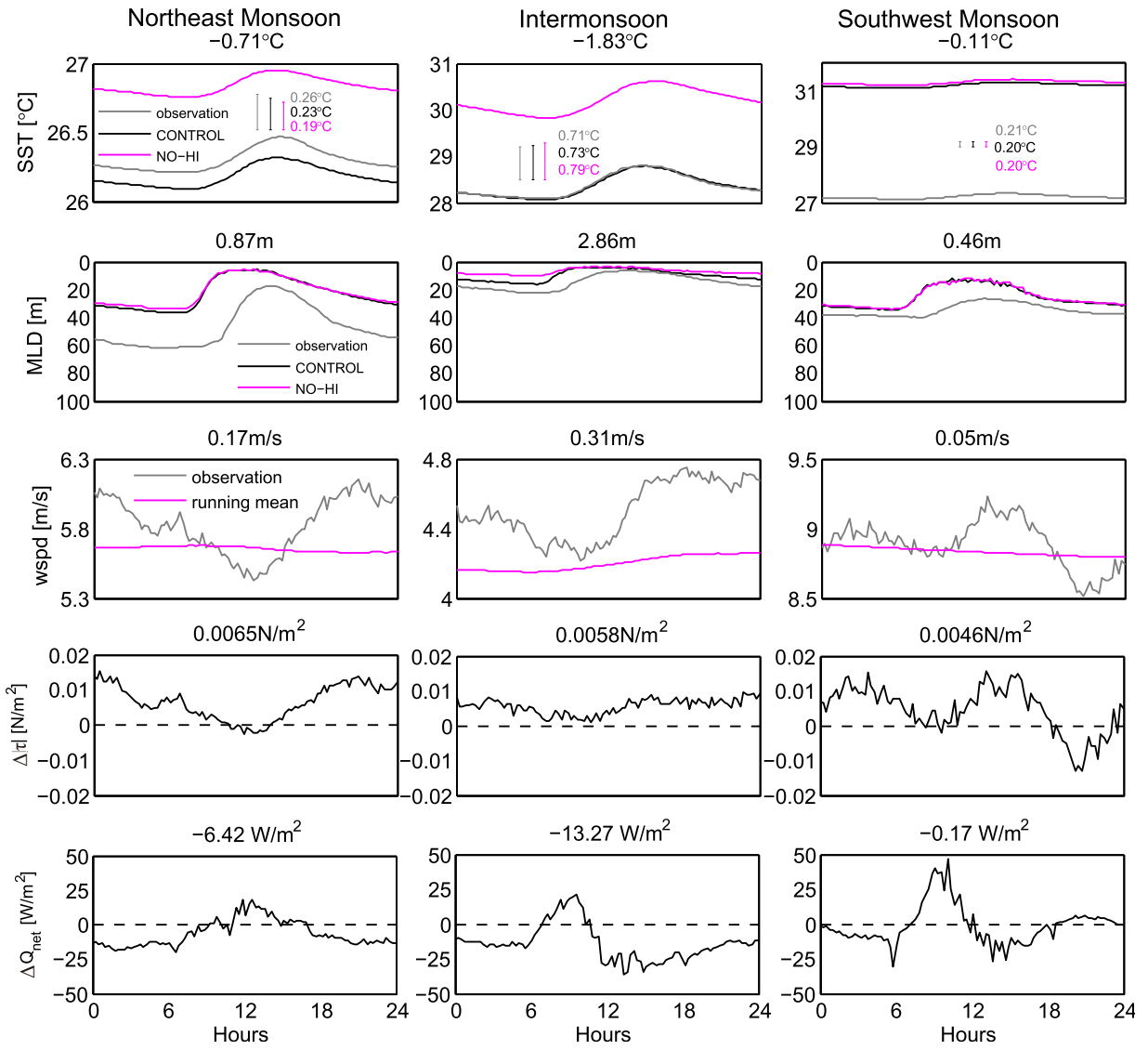

Figure 4. A 24 h composite view of (top) SST, (second row) ML depth, and (middle) wind speed showing observations (grey), CONTROL (black), and NO-HI (magenta) experiments. The next two rows show differences in (fourth row) wind stress and (bottom) net surface heat fluxes between the CONTROL and NO-HI. The composites are for three seasons: (left) the NE monsoon, (middle) the intermonsoon, and (right) the SW monsoon. Values of seasonal-mean differences (CONTROL – NO-HI) are shown at the top of each figure. The composite-averaged magnitude of SST diurnal variability simulated by the CONTROL and NO-HI are illustrated in the top figures. Note that different axis limits are used in different seasons for the composites of SST, ML depth, and wind speed.

in turbulent heat flux owing to high-frequency wind fluctuations, with the difference in radiative heat flux owing to high-frequency cloud variability making only a small contribution (Figure 5).

Second, the background ML depth modulates the SST response to the high-frequency atmospheric forcing seasonally due to its seasonal variation. As shown in Figure 2e, both the observed and model-simulated ML is much shallower in the intermonsoon season (typically 15 m in observation) than in monsoon seasons (40–50 m in the observations). The effect of seasonally dependent ML depth in modulating the impact of high-frequency weather systems is more readily seen by comparing the results from WIND and NO-HI. In both experiments, the impact of high-frequency weather systems on surface heat fluxes is excluded, i.e., without the first contributing factor. While the wind stress differences between WIND and NO-HI are comparable among all three seasons (∼0.005 N/m^2; see also Figure 4), the cooling effect on the SST is much greater in the intermonsoon season (Figure 2c), because the shallower surface ML in the intermonsoon season, via its smaller heat capacity, amplifies the cooling effect induced by the stronger shear instability and enhanced entrainment by including the high-frequency wind fluctuations.

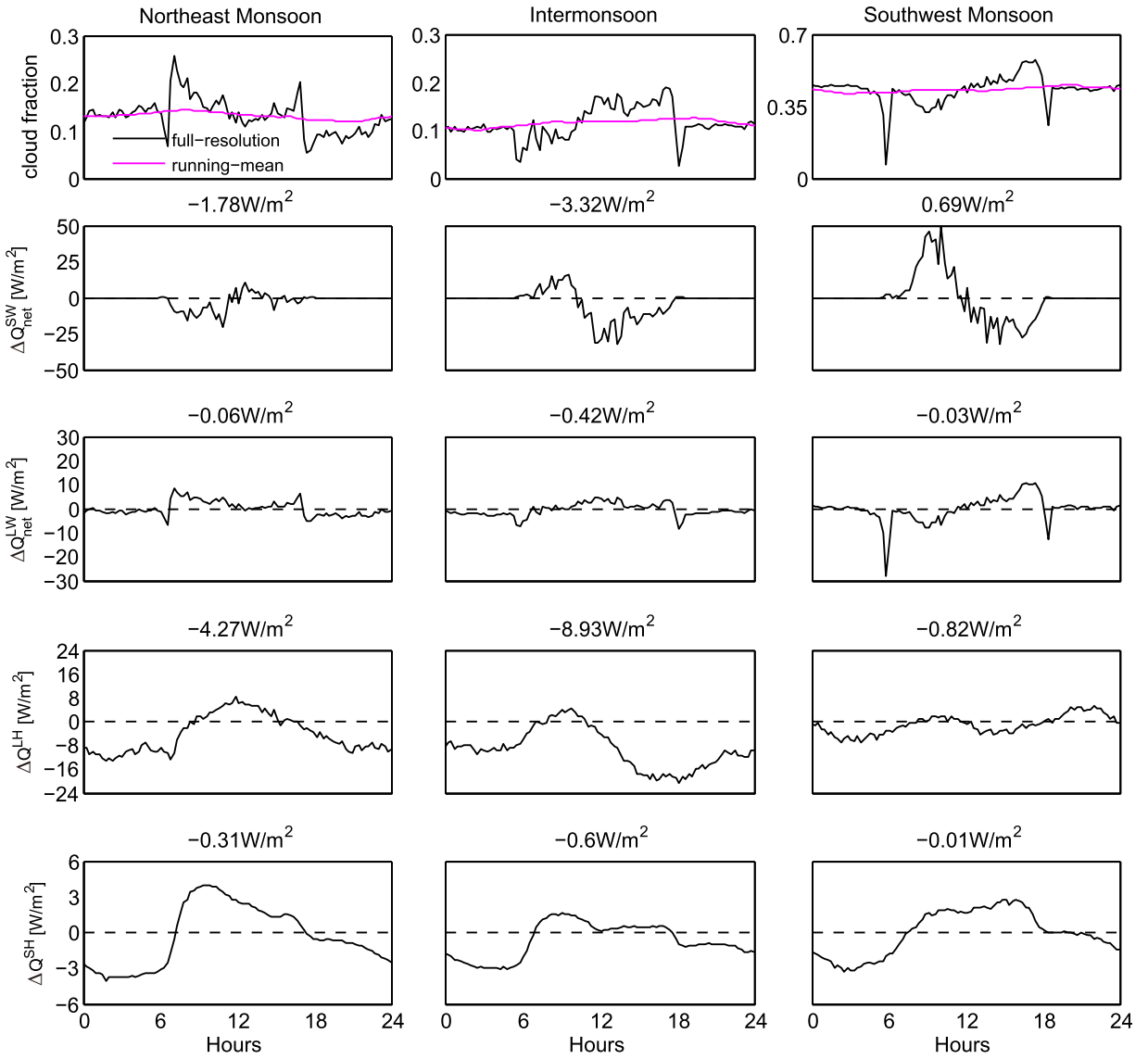

Figure 5. The 24 h composite view of subdaily (black) and daily-averaged (magenta) cloud cover and the difference of net surface shortwave radiation (Q_{net}^{SW}), longwave radiation (Q_{net}^{LW}), latent heat flux (Q^{LH}), and sensible heat flux (Q^{SH}) between the CONTROL and NO-HI experiments in the (left) NE monsoon, (middle) intermonsoon, and (right) SW monsoon seasons. Values of seasonal-mean differences (CONTROL – NO-HI) are shown on the top of each figure. Note that different axis limits are used in different seasons for the composite cloud fraction.

The composite analysis also provides a closer look at the impact of high-frequency weather systems on the SST diurnal variability. Our results show that high-frequency cloud variability (Figure 5) and high-frequency wind variability (Figure 4) at the study site have no clear and significant diurnal cycle, except for in wind speed during the NE monsoon season, which is a modest 0.4 m/s. As such, filtering out high-frequency cloud and wind variability does not significantly alter the diurnal cycles of solar radiation and wind-induced vertical mixing and entrainment. Consequently, high-frequency weather systems are found to have little systematic effect on the magnitude of the SST diurnal variability at this site.

3.4. Role of High-Frequency Wind Fluctuations

The bulk flux formulae (equation (1)) show that the surface winds (**U**) are involved not only in the wind stress but also in the turbulent heat fluxes calculations. The impact of the high-frequency wind gusts on the turbulent heat fluxes is shown in the composite analysis, which suggests that the wind-related turbulent heat fluxes are the major contribution to the difference in the net surface heat fluxes between the CONTROL (high-frequency) and the NO-HI (low-frequency) experiments.

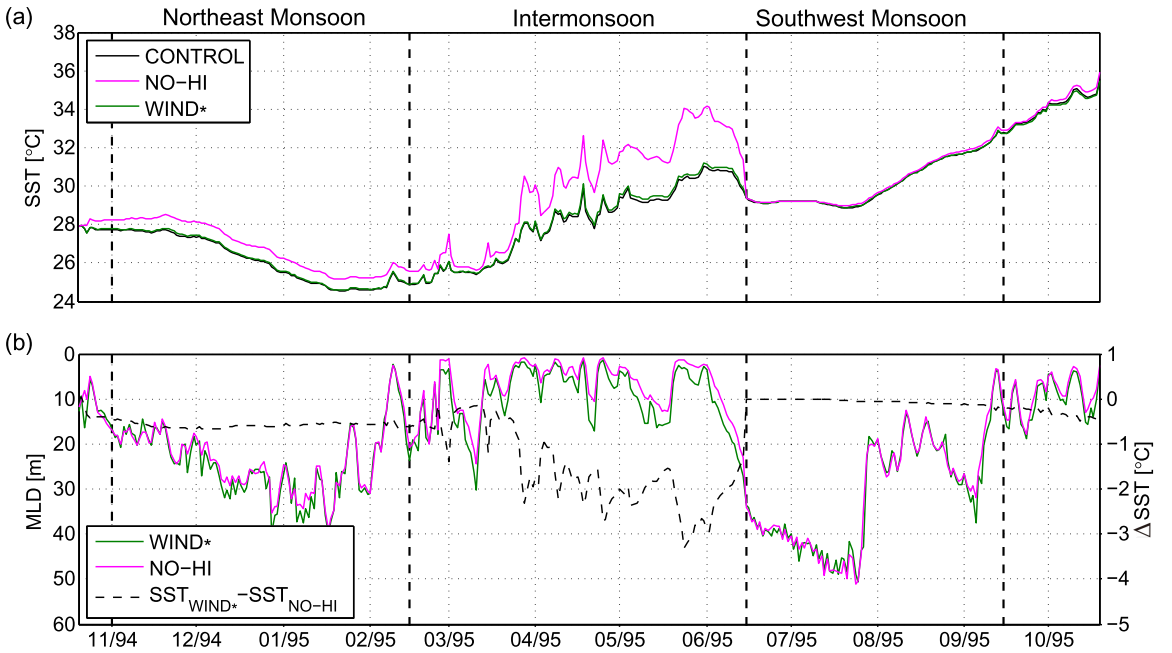

Figure 6. (a) Daily-mean SST from the CONTROL (black), NO-HI (magenta), and WIND* (green) experiments. (b) Daily-mean ML depth in the NO-HI and WIND* experiments and daily-mean SST difference (dashed) between the two experiments (WIND* – NO-HI).

To investigate the net effect of high-frequency wind fluctuations on modulating the SST evolution and ML depth, an extra experiment WIND* is conducted, with a new forcing which applies full-resolution winds but other meteorological variables daily averaged. The simulated SST evolves closely to the CONTROL simulation (Figure 6a) as expected, since the high-frequency wind explains most of the high-frequency variability in the atmospheric forcing via both the momentum and turbulent heat fluxes. The increased turbulent heat loss and enhanced wind-driven shear instability caused by including high-frequency wind variability (Brannigan et al., 2013; Lincoln et al., 2016) lead to cooler SST and a deeper the ML depth in the WIND* experiment in comparison with the NO-HI experiment. Our results also show that the magnitude of the SST difference between WIND* and NO-HI is tightly linked to the background ML depth on a day-to-day time scale during the intermonsoon season when the ML depth is shallow (Figure 6b). Similar to the mechanism of ML seasonal regulation on the SST difference between NO-HI and CONTROL, as discussed in the previous section, during the intermonsoon season, most of the variability of ML thermal anomalies induced by enhanced entrainment and turbulent heat loss are reflected on the SST field due to the smaller heat capacity of shallower ML depth. Such linkage between SST difference and ML variability is absent in both the monsoon seasons, as the heat anomalies are evenly distributed over a deeper ML in the model and thus the thermal variability reflected on the SST field is largely damped.

4. Summary and Conclusions

We have investigated the impact of high-frequency (subdaily time scale) weather systems on SST and ML depth using the one-dimensional PWP model and an observational data set collected in the central Arabian Sea. By comparing model simulations that include, partially include, and exclude atmospheric forcing associated with high-frequency weather systems, we find the following:

1. High-frequency weather systems lower the daily-mean SST by 0.8°C on average (and as much as 3.7°C) and damp its variability but have little systematic effect on the diurnal variability of SST. This is in sharp contrast to the effect of diurnal air-sea fluxes which act to increase the daily-mean SST via a rectification effect of a thin warm surface layer formed during the day. The difference in the SST between filtering the meteorological variables and filtering the fluxes was up to 4°C in the central Arabian Sea.
2. The magnitude of the SST's response to high-frequency weather systems is strongly regulated by the background ML depth on daily-to-seasonal time scales. There is a greater response in SST during the

intermonsoon season, when the ML depth is shallow, compared to the response in the monsoon seasons. Implicitly our results show an interesting link across time scales. High-frequency meteorological forcing impacts the ML depth, while low-frequency (seasonal) changes in the ML depth dictate the magnitude of the SST response.

3. High-frequency weather systems impact the SST and surface ML at this site primarily through fluctuations in the wind field via their influence of the wind stress and turbulent heat flux. The seasonal feature of the wind fluctuations (intermonsoon winds blowing unevenly while monsoon winds blowing uniformly in direction) results in greater wind speed changes in the intermonsoon season caused by the daily averaging of the winds, and thus leads to greater air-sea fluxes changes, which contributes to the greater responses of SST and ML depth.

This study illustrates a distinct seasonal cycle in the oceanic response to high-frequency weather systems under different monsoonal forcings over a typical year in the central Arabian Sea. The generic setup of our experiments suggests our findings are likely to be applicable to other tropical seas with similar monsoon-dominated atmospheric conditions.

Appendix A: The KC Model Validation

As an alternative to the PWP model, we repeated our simulations with a turbulence closure model, the Kantha-Clayson (KC) model (Kantha & Clayson, 1994). The results are broadly similar to those from the PWP

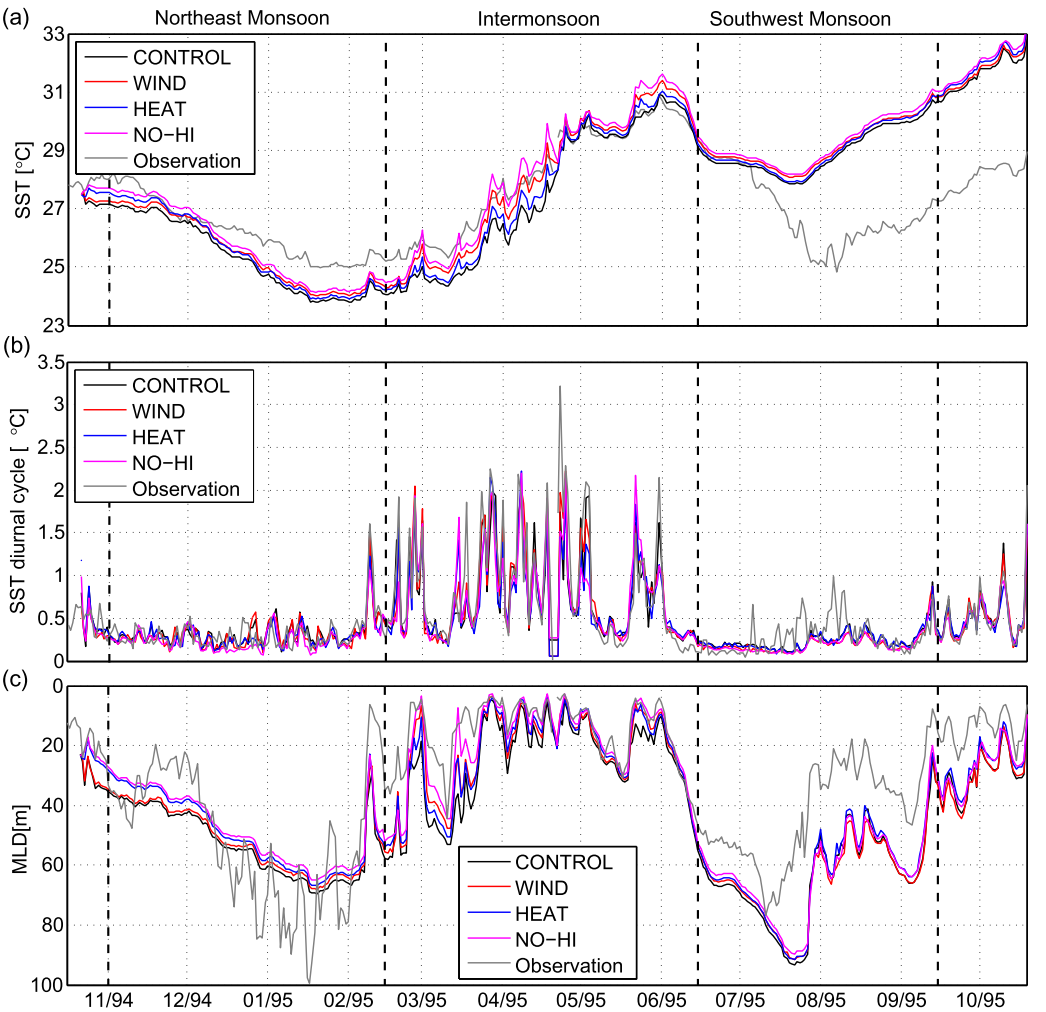

Figure A1. Yearlong time series of (a) daily-mean SST, (b) magnitude of SST diurnal variability, and (c) daily-mean ML depth. The line colors show observation (grey) and the KC model simulations: CONTROL (black), WIND (red), HEAT (blue), and NO-HI (magenta).

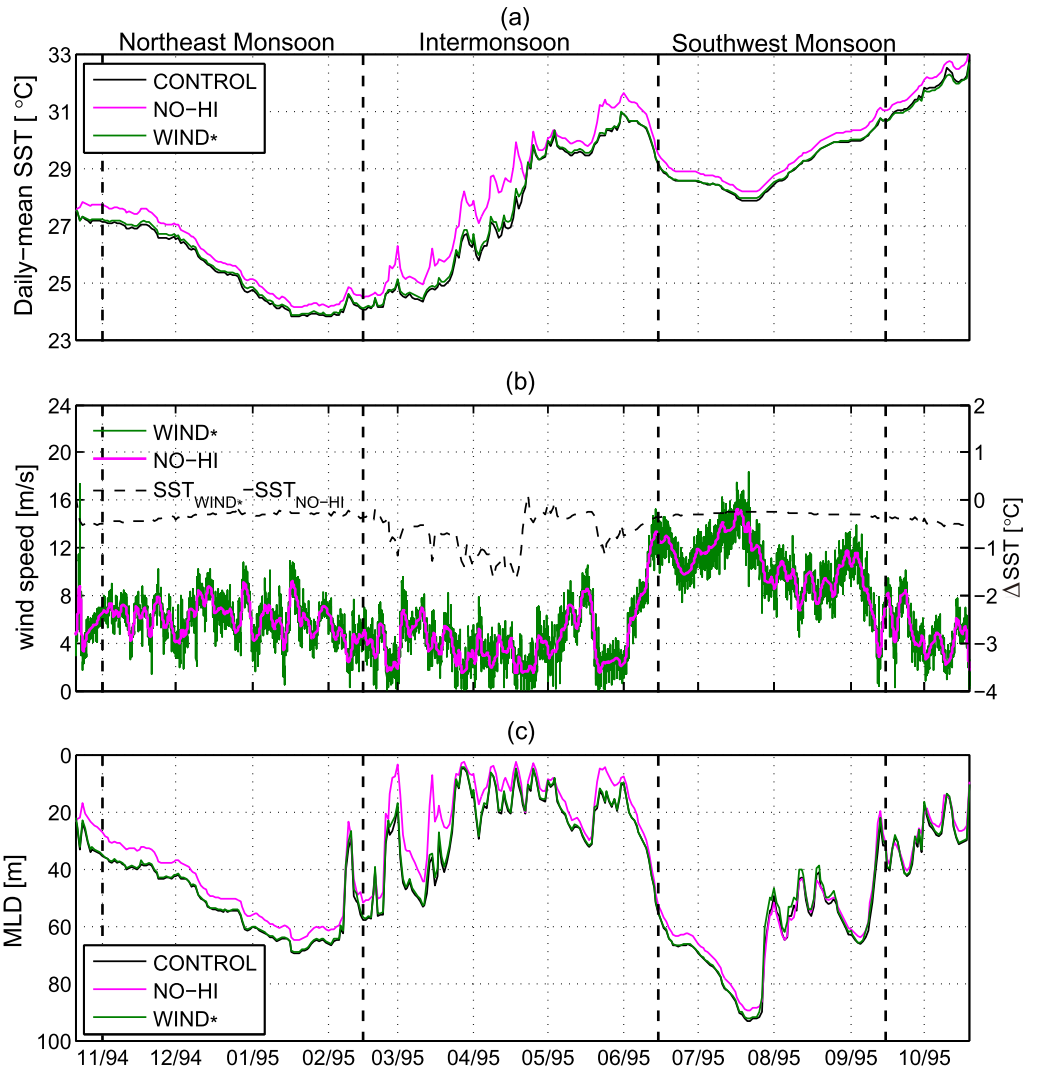

Figure A2. (a) Daily-mean SST for the CONTROL (black), NO-HI (magenta), and WIND* (green) experiments. (b) Wind speed used in NO-HI and WIND* and daily-mean SST difference (dashed) between the two experiments (WIND* – NO-HI). (c) Daily-mean ML depth in the CONTROL, NO-HI, and WIND* experiments.

model (see Figures A1 and A2). The KC model has captured the major role played by high-frequency weather systems—deepening the ML, lowering the low-frequency SST, and damping its variability, without systematically altering the SST diurnal variability. By comparing the simulated SST, the magnitude of SST

Table A1
Comparison of the Magnitude of SST Diurnal Variability in Observations and Simulations Using the PWP Model and the KC Model

	Magnitude of diurnal variability in SST (°C)			
Integration	Mean	Max	Min	STD
	PWP/KC	PWP/KC	PWP/KC	PWP/KC
CONTROL	0.44/0.52	3.33/2.30	0.04/0.11	0.53/0.42
WIND	0.43/0.51	3.35/2.44	0.04/0.09	0.51/0.45
HEAT	0.43/0.50	3.33/2.28	0.04/0.10	0.50/0.41
NO-HI	0.45/0.45	3.40/2.42	0.04/0.07	0.57/0.41
Observation	0.54	2.29	0.04	0.59

diurnal variability and the ML depth between KC and PWP simulations, it is concluded that the mixing process is enhanced in the KC model. In the KC model, the simulated SST is somehow lower than observations in the NE monsoon season, and the drift between model simulation and observations takes place at the onset of southwesterly burst as we find in PWP predictions. The simulated ML depth in CONTROL is generally deeper than that in PWP by 18 m on average. The ML depth in the KC model reaches down to 50 m in the intermonsoon season and nearly 100 m in the SW monsoon season. The magnitude of the SST diurnal variability is also smaller than the PWP (Table A1). All these comparisons indicate that the mixing processes parameterized in KC model is stronger than that in PWP model. Despite of the difference in the strength of vertical mixing, it is robust that the high-frequency wind variability is the major contribution to the changes of air-sea heat and momentum fluxes due to the high-frequency weather systems at this site. The response of SST to high-frequency weather systems in the KC model is not as closely correlated to the background ML depth on daily time scale during the intermonsoon season as that found in the PWP model since the high-frequency variability in SSTs are damped by the deeper ML depth in the KC simulations. The seasonal correspondence between the ML depth and either SST response or the magnitude of SST diurnal variability still exists. The broad agreement between results from the KC model and PWP model lends confidence on the robustness of the findings of this study.

Acknowledgments

Shenjie Zhou thanks Robert Weller and Kelan Huang for their helpful discussion on the central Arabian Sea data set and for sharing the updated COARE bulk formulae used in this study. Shenjie Zhou also thanks Alec Bogdanoff for the help with the KC model. We thank Adrian Matthews for useful discussions. We thank two anonymous reviewers for their constructive comments that led to a much improved manuscript. The Arabian Sea site data set was collected and processed by the Upper Ocean Process Group in Woods Hole Oceanographic Institute (UOP-WHOI). The data are available at http://uop.whoi.edu/projects/arabiansea/arabiansea.html.

References

Ångström, A. (1915). A study of the radiation of the atmosphere. In *Smithsonian miscellaneous collection* (Vol. 65, 182 pp.). Washington, DC: Smithsonian Institution.

ASCE-EWRI. (2005). *The ASCE standardized reference evapotranspiration equation* (173 pp.). Reston, VA: American Society of Civil Engineers.

Bender, M. A., Ginis, I., & Kurihara, Y. (1993). Numerical simulations of tropical cyclone-ocean interaction with a high-resolution coupled model. *Journal of Geophysical Research: Atmospheres*, *98*(D12), 23245. https://doi.org/10.1029/93JD02370

Bernie, D. J., Guilyardi, E., Madec, G., Slingo, J. M., & Woolnough, S. J. (2007). Impact of resolving the diurnal cycle in an ocean-atmosphere GCM. Part 1: A diurnally forced OGCM. *Climate Dynamics*, *29*(6), 575–590. https://doi.org/10.1007/s00382-007-0249-6

Bernie, D. J., Guilyardi, E., Madec, G., Slingo, J. M., Woolnough, S. J., & Cole, J. (2008). Impact of resolving the diurnal cycle in an ocean-atmosphere GCM. Part 2: A diurnally coupled CGCM. *Climate Dynamics*, *31*(7–8), 909–925. https://doi.org/10.1007/s00382-008-0429-z

Bernie, D. J., Woolnough, S. J., Slingo, J. M., & Guilyardi, E. (2005). Modeling diurnal and intraseasonal variability of the ocean ML. *Journal of Climate*, *18*(8), 1190–1202. https://doi.org/10.1175/JCLI3319.1

Brannigan, L., Lenn, Y., Rippeth, T. P., McDonagh, E., Chereskin, T. K., & Sprintall, J. (2013). Shear at the base of the oceanic mixed layer generated by wind shear alignment. *Journal of Physical Oceanography*, *43*, 1798–1810. https://doi.org/10.1175/JPO-D-12-0104.1

Brunt, D. (1932). Notes on radiation in the atmosphere. I. *Quarterly Journal of the Royal Meteorological Society*, *58*(247), 389–420. https://doi.org/10.1002/qj.49705824704

Brutsaert, W. (1975). On a derivable formula for long-wave radiation from clear skies. *Water Resources Research*, *11*(5), 742–744. https://doi.org/10.1029/WR011i005p00742

Condron, A., Bigg, G. R., & Renfrew, I. A. (2008). Modeling the impact of polar mesocyclones on ocean circulation. *Journal of Geophysical Research: Oceans*, *113*, C10005. https://doi.org/10.1029/2007JC004599

Condron, A., & Renfrew, I. A. (2013). The impact of polar mesoscale storms on northeast Atlantic Ocean circulation. *Nature Geoscience*, *6*(1), 34–37. https://doi.org/10.1038/ngeo1661

Danabasoglu, G., Large, W. G., Tribbia, J. J., Gent, P. R., Briegleb, B. P., & McWilliams, J. C. (2006). Diurnal coupling in the tropical oceans of CCSM3. *Journal of Climate*, *19*(11), 2347–2365. https://doi.org/10.1175/JCLI3739.1

Dare, R. A., & McBride, J. L. (2011). Sea surface temperature response to tropical cyclones. *Monthly Weather Review*, *139*(12), 3798–3808. https://doi.org/10.1175/MWR-D-10-05019.1

Dilley, A. C., & O'Brien, D. M. (1997). Estimating downward clear sky long-wave irradiance at the surface from screen temperature and precipitable water. *Quarterly Journal of the Royal Meteorological Society*, *124*(549), 1391–1401. https://doi.org/10.1002/qj.49712454903

Fairall, C. W., Bradley, E. F., Hare, J. E., Grachev, A. A., & Edson, J. B. (2003). Bulk parameterisation of air-sea fluxes: Updates and verification for the COARE algorithm. *Journal of Climate*, *16*(4), 571–591. https://doi.org/10.1175/1520-0442(2003)016<0571:BPOASF>2.0.CO;2

Findlater, J. (1977). Observational aspects of the low-level cross-equatorial jet stream of the western Indian Ocean. *Pure and Applied Geophysics*, *115*(5–6), 1251–1262. https://doi.org/10.1007/BF00874408

Fischer, A. S. (2000). *The upper ocean response to the monsoon in the Arabian Sea* (PhD thesis, 220 pp.). Woods Hole: Massachusetts Institute of Technology and Woods Hole Oceanographic Institution.

Fischer, A. S., Weller, R. A., Rudnick, D. L., Eriksen, C. C., Lee, C. M., Brink, K. H., et al. (2002). Mesoscale eddies, coastal upwelling, and the upper-ocean heat budget in the Arabian Sea. *Deep Sea Research Part II: Topical Studies in Oceanography*, *49*(12), 2231–2264. https://doi.org/10.1016/S0967-0645(02)00036-X

Gubler, S., Gruber, S., & Purves, R. S. (2012). Uncertainties of parameterised surface downward clear-sky shortwave and all-sky longwave radiation. *Atmospheric Chemistry and Physics*, *12*(11), 5077–5098. https://doi.org/10.5194/acp-12-5077-2012

Gulev, S. K., & Belyaev, K. (2012). Probability distribution characteristics for surface air-sea turbulent heat fluxes over the global ocean. *Journal of Climate*, *25*(1), 184–206. https://doi.org/10.1175/2011JCLI4211.1

Ham, S., Hong, S. Y., & Park, S. (2014). A study on air-sea interaction on the simulated seasonal climate in an ocean-atmosphere coupled model. *Climate Dynamics*, *42*(5–6), 1175–1187. https://doi.org/10.1007/s00382-013-1847-0

Holdsworth, A. M., & Myers, P. G. (2015). The influence of high-frequency atmospheric forcing on the circulation and deep convection of the Labrador Sea. *Journal of Climate*, *28*(12), 4980–4996. https://doi.org/10.1175/JCLI-D-14-00564.1

Hu, W., Duan, A., & Wu, G. (2015). Impact of subdaily air-sea interaction on simulating intraseasonal oscillations over the tropical Asian monsoon region. *Journal of Climate*, *28*(3), 1057–1073. https://doi.org/10.1175/JCLI-D-14-00407.1

Idso, S. B. (1981). A set of equations for full spectrum and 8- to 14 micron and 10.5- to 12.5 micron thermal radiation from cloudless skies. *Water Resources Research*, *17*(2), 295–304. https://doi.org/10.1029/WR017i002p00295

Idso, S. B., & Jackson, R. D. (1969). Thermal radiation from the atmosphere. *Journal of Geophysical Research*, *74*(23), 5397. https://doi.org/10.1029/JC074i023p05397

Iziomon, M. G., Mayer, H., & Matzarakis, A. (2003). Downward atmospheric longwave irradiance under clear and cloudy skies: Measurement and parameterisation. *Journal of Atmospheric and Solar-Terrestrial Physics*, *65*(10), 1107–1116. https://doi.org/10.1016/j.jastp.2003.07.007

Jung, T., Serrar, S., & Wang, Q. (2014). The oceanic response to mesoscale atmospheric forcing. *Geophysical Research Letters*, *41*, 1255–1260. https://doi.org/10.1002/2013GL059040

Kantha, L. H., & Clayson, C. A. (1994). An improved ML model for geophysical applications. *Journal of Geophysical Research: Oceans*, *99*(C12), 25235. https://doi.org/10.1029/94JC02257

Konzelmann, T., van de Wal, R. S. W., Greuell, W., Bintanja, R., Henneken, E. A. C., & Abe-Ouchi, A. (1994). Parameterization of global and longwave incoming radiation for the Greenland Ice Sheet. *Global and Planetary Change*, *9*(1–2), 143–164. https://doi.org/10.1016/0921-8181(94)90013-2

Lincoln, B. J., Rippeth, T. P., & Simpson, J. H. (2016). Surface mixed layer deepening through wind shear alignment in a seasonally stratified shallow sea. *Journal of Geophysical Research: Oceans*, 121. https://doi.org/10.1002/2015JC011382

Maykut, G. A., & Church, P. E. (1973). Radiation climate of Barrow Alaska, 1962-66. *Journal of Applied Meteorology*, *12*, 620–628. https://doi.org/10.1175/1520-0450(1973)012<0620:RCOBA>2.0.CO;2

Prata, A. J. (1996). A new long-wave formula for estimating downward clear-sky radiation at the surface. *Quarterly Journal of the Royal Meteorological Society*, *122*(533), 1127–1151. https://doi.org/10.1002/qj.49712253306

Price, J. F., Morzel, J., & Niiler, P. P. (2008). Warming of SST in the cool wake of a moving hurricane. *Journal of Geophysical Research: Oceans*, *113*, C07010. https://doi.org/10.1029/2007JC004393

Price, J. F., Weller, R. A., & Pinkel, R. (1986). Diurnal cycling: Observations and models of the upper ocean response to diurnal heating, cooling, and wind mixing. *Journal of Geophysical Research: Oceans*, *91*(C7), 8411–8427. https://doi.org/10.1029/JC091iC07p08411

Reed, R. (1977). On estimating insolation over the ocean. *Journal of Physical Oceanography*, *7*, 482–485. https://doi.org/10.1175/1520-0485(1977)007<0482:OEIOTO>2.0.CO;2

Satterlund, D. R. (1979). An improved equation for estimating longwave radiation from the atmosphere. *Water Resources Research*, *15*(6), 1649–1650. https://doi.org/10.1029/WR015i006p01649

Shinoda, T. (2005). Impact of the diurnal cycle of solar radiation on intraseasonal SST variability in the western equatorial Pacific. *Journal of Climate*, *18*(14), 2628–2636. https://doi.org/10.1175/JCLI3432.1

Shinoda, T., & Hendon, H. H. (1998). ML modeling of intraseasonal variability in the tropical western Pacific and Indian Oceans. *Journal of Climate*, *11*(10), 2668–2685. https://doi.org/10.1175/1520-0442(1998)011<2668:MLMOIV>2.0.CO;2

Swinbank, W. C. (1963). Long-wave radiation from clear skies. *Journal of Applied Meteorology*, *89*(381), 339–348. https://doi.org/10.1002/qj.49708938105

Terray, P., Kamala, K., Masson, S., Madec, G., Sahai, A. K., Luo, J. J., et al. (2012). The role of the intra-daily SST variability in the Indian monsoon variability and monsoon-ENSO-IOD relationships in a global coupled model. *Climate Dynamics*, *39*(3), 729–754. https://doi.org/10.1007/s00382-011-1240-9

Våge, K., Pickart, R. S., Moore, G. W. K., & Ribergaard, M. H. (2008). Winter mixed layer development in the central Irminger Sea: The effect of strong, intermittent wind events. *Journal of Physical Oceanography*, *38*(3), 541–565. https://doi.org/10.1175/2007JPO3678.1

Weller, R. A., Baumgartner, M. F., Josey, S. A., Fischer, A. S., & Kindle, J. C. (1998). Atmospheric forcing in the Arabian Sea during 1994–1995: Observations and comparisons with climatology and models. *Deep Sea Research Part II: Topical Studies in Oceanography*, *45*(10–11), 1961–1999. https://doi.org/10.1016/S0967-0645(98)00060-5

Weller, R. A., Fischer, A. S., Rudnick, D. L., Eriksen, C. C., Dickey, T. D., Marra, J., et al. (2002). Moored observations of upper-ocean response to the monsoons in the Arabian Sea during 1994–1995. *Deep Sea Research Part II: Topical Studies in Oceanography*, *49*(12), 2195–2230. https://doi.org/10.1016/S0967-0645(02)00035-8

Wu, Y., Zhai, X., & Wang, Z. (2016). Impact of synoptic atmospheric forcing on the mean ocean circulation. *Journal of Climate*, *29*(16), 5709–5724. https://doi.org/10.1175/JCLI-D-15-0819.1

Zhai, X., Johnson, H. L., Marshall, D. P., & Wunsch, C. (2012). On the wind power input to the ocean general circulation. *Journal of Physical Oceanography*, *42*(8), 1357–1365. https://doi.org/10.1175/JPO-D-12-09.1

Zhai, X., & Wunsch, C. (2013). On the variability of wind power input to the oceans with a focus on the subpolar North Atlantic. *Journal of Climate*, *26*(11), 3892–3903. https://doi.org/10.1175/JCLI-D-12-00472.1

Zillman, J. W. (1972). *A study of some aspects of the radiation and heat budgets of the Southern Hemisphere oceans. Meteorological studies, 26* (562 pp.). Canberra, Australia: Bureau of Meteorology, Department of the Interior.